Small-scale Testing of Bucket Foundations in Sand

Knudsen, Bjørn S.; Østergaard, Martin Underlin; Ibsen, Lars Bo

Publication date:
2013

Document Version
Publisher's PDF, also known as Version of record

Small-scale Testing of Bucket Foundations in Sand

Bjørn Staghøj Knudsen
Martin Underlin Østergaard
Lars Bo Ibsen

DEPARTMENT OF CIVIL ENGINEERING
AALBORG UNIVERSITY

ISSN 1901-7278
DCE Technical Memorandum No. 33

Aalborg University
Department of Civil Engineering

DCE Technical Memorandum No. 33

Small-scale Testing of Bucket Foundations in Sand

by

Bjørn Staghøj Knudsen
Martin Underlin Østergaard
Lars Bo Ibsen

June 2013

Scientific Publications at the Department of Civil Engineering

Technical Reports are published for timely dissemination of research results and scientific work carried out at the Department of Civil Engineering (DCE) at Aalborg University. This medium allows publication of more detailed explanations and results than typically allowed in scientific journals.

Technical Memoranda are produced to enable the preliminary dissemination of scientific work by the personnel of the DCE where such release is deemed to be appropriate. Documents of this kind may be incomplete or temporary versions of papers—or part of continuing work. This should be kept in mind when references are given to publications of this kind.

Contract Reports are produced to report scientific work carried out under contract. Publications of this kind contain confidential matter and are reserved for the sponsors and the DCE. Therefore, Contract Reports are generally not available for public circulation.

Lecture Notes contain material produced by the lecturers at the DCE for educational purposes. This may be scientific notes, lecture books, example problems or manuals for laboratory work, or computer programs developed at the DCE.

Theses are monograms or collections of papers published to report the scientific work carried out at the DCE to obtain a degree as either PhD or Doctor of Technology. The thesis is publicly available after the defence of the degree.

Latest News is published to enable rapid communication of information about scientific work carried out at the DCE. This includes the status of research projects, developments in the laboratories, information about collaborative work and recent research results.

Published 2013 by
Aalborg University
Department of Civil Engineering
Sohngaardsholmsvej 57,
DK-9000 Aalborg, Denmark

Printed in Aalborg at Aalborg University

ISSN 1901-7278
DCE Technical Memorandum No. 33

Small-scale Testing of Bucket Foundations in Sand

Bjørn Staghøj Knudsen[1] Martin Underlin Østergaard[1] Lars Bo Ibsen[2]

Department of Civil Engineering, Aalborg University

Abstract

For offshore foundation structures, the loads are of varying nature both in magnitude and duration. For the bucket foundation the dissipation of the pore pressure is highly relevant since it greatly affects the strength of the structure. The build up of pore pressures with varying loading rate is therefore a highly relevant research subject. In computational models, e.g. FE-models, normally either a drained or an undrained behaviour is assumed. In real life, the behaviour is partially drained, which calls for a time-dependent model. Especially, the tracking of pore pressures in and around the bucket skirt will provide valuable information of the quasi-static behaviour. For a number of small-scale tests performed in the laboratory at Aalborg University, a bucket foundation will be loaded with varying velocity to investigate the dissipation and general behaviour of bucket foundations used as offshore support structures for wind turbines.

1 Introduction

The suction bucket concept for offshore foundation of wind turbines, which is illustrated in figure 1, has been extensively researched for the last decade, among other places at the Geotechnics Department of Aalborg University (AAU). The design procedure and validation of the foundation dimensions have to be verified by risk assessment organizations such as *Det Norske Veritas*. In the current verified design method the ultimate capacity of the bucket foundation is calculated both in the drained and undrained condition whereafter the lowest capacity is chosen. In dense cohesionless soil the response in the drained case will often be significantly lower than the undrained, causing the capacity to be low. As the ultimate limit state loads on offshore structures are often of impulsive nature, i.e. a very large load over a small period of time, arising from emergency stop of the turbine, freak waves or breaking waves in general, this article aims to investigate the behaviour of the foundation as a function of the loading rate. The thesis is that for large loading rates, the drained condition is an underestimation of the capacity of the foundation, causing the design dimension to be overestimated.

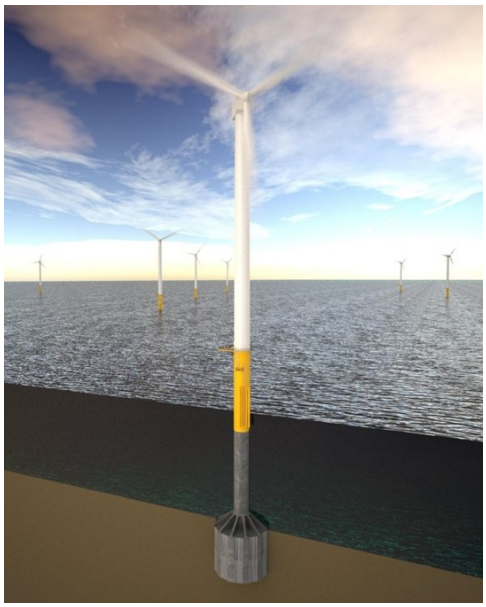

Figure 1: An illustration of a wind turbine on a bucket foundation. (Universal Foundation A/S, 2013)

The thesis has previously been investigated by conducting tests in the pressure tank at the Geotechnics Laboratory at AAU, cf. (Sjelmo et al., 2012) and (Foglia et al., 2013) among others. The thesis was in these tests validated, however the test setup was not able to conduct the test to a satisfactory degree, mainly due to a limited displacement range of 40 mm of the piston, cf. figure 4. Since the before mentioned tests were conducted, the test setup has been thoroughly upgraded. The upgrade involves a new actuator, new bucket foundations with greater steel thickness and an addition of five extra pore pressure gauges. Furthermore new control hard- and software has been installed. With the new setup it is possible to exert much larger forces at greater velocities over a larger displacement range. In this article the results of the first four successful tests with the new setup will be analyzed and compared to the previously obtained results.

[1] *M.Sc. Student, Department of Civil Engineering, Aalborg University, Denmark*

[2] *Professor, Department of Civil Engineering, Aalborg University, Denmark*

2 Theory

The sand in the pressure tank is Aalborg University Sand no. 1, which is thoroughly documented from triaxial tests. The sand resembles sand types commonly encountered offshore. For the calculation of failure sand is defined as being in either a drained or undrained state, representing the two extremes of drainage behaviour. In the tests it is investigated what happens as a transition from fully drained conditions at low loading velocity to a potentially partial or fully undrained behaviour at high loading velocities occurs. A partially undrained behaviour can be experienced when a pore pressure build up is not able to dissipate, which makes the behaviour a function of the drainage conditions and the permeability of the soil.

2.1 Development of Pore Pressures

Sand under drained conditions can act both compressional with $\Delta\varepsilon_V < 0$ and dilatational with $\Delta\varepsilon_V > 0$ under loading. The change between the two states is called the characteristic state and is characterized by,

$$\frac{\delta\varepsilon_V}{\delta\varepsilon_1} = 0. \tag{1}$$

The point of the characteristic state for different density indices and stress combinations can be plotted in a $p' - q$ diagram where they form a straight line. This line is called the characteristic line, cf. (Ibsen and Lade, 1997). Sand with stress states below the line thus exhibits compression and stress states above exhibits dilatation. The slope of the characteristic line is called the characteristic angle ϕ_{cl}, and this angle has for Aalborg University Sand no. 1 been found to be independent of the density index, cf. Ibsen and Lade (1998). A schematic overview of the drained behaviour can be seen in figure 2. For the sand to behave fully drained the effective stress path (ESP) and the total stress path (TSP) have to be coincident, as seen in figure 2. This only takes place if the excessive pore pressure formed during volume change of the sand is able to dissipate, which in turn requires the loading rate to be low.

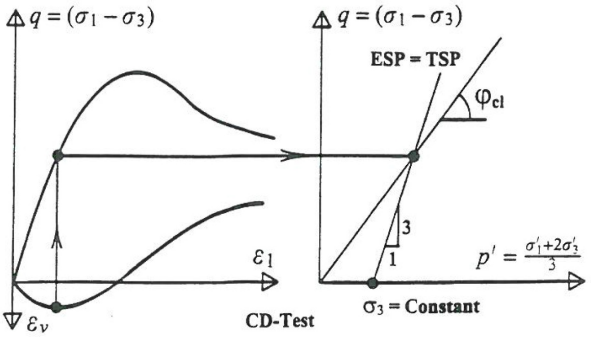

Figure 2: The characteristic state in drained sand. (Ibsen and Lade, 1997)

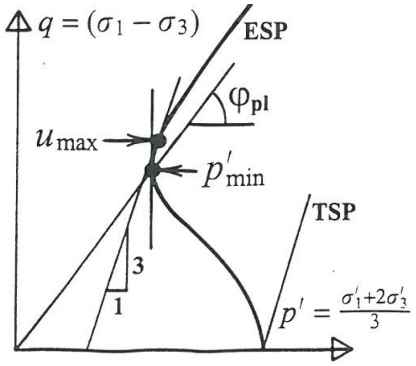

Figure 3: The phase transformation state in undrained sand. (Ibsen and Lade, 1997)

For sand in the undrained state a similar property is seen as the point at which the pore pressure development Δu changes from being positive to negative. This change is associated with compression and dilation of sand in drained behaviour. The state at which the transition takes place is called the phase transformation state, cf. (Ibsen and Lade, 1997). As with the drained case the phase transformation line is a straight line in a $p' - q$ diagram, cf. figure 3. The phase transition point is defined as the point at which the ESP has a vertical tangent, since the point of maximum pore pressure u_{max} and minimum effective mean stress does not completely align, cf. figure 3. Once the pore pressure increment is negative the effective pressure state will increase, thus giving the soil extra strength. A sand with a highly dilatational behaviour will therefore have a higher strength. The negative pore pressure increment prevents the sand from dilating as long as the pore pressure is positive, once the pore pressure turns negative, the sand starts to dilate and is no longer fully undrained. As the pore pressure nears the point of cavitation the failure is controlled by the drained failure envelope.

Since the failure point of dense undrained sand occurs once the pore pressure reaches the cavitation limit, the value of the pore pressure in the initial state is important for the total strength. In the undrained state it is thus the total stress state $p' + u_0$ that is relevant for the strength, and not the effective stress as for the drained case. The combination of u_0 and p' is furthermore not relevant, only the sum. As a consequence for the sand in the pressure tank, the undrained ultimate capacity will be greatly increased due to the pressure applied, even though the effective stresses are not changed. (Nielsen et al., 2013)

Whether or not the sand will act drained or undrained is a function of the drainage conditions, the permeability of the sand and the loading rate. It has often been found that a high loading rate in saturated sand will cause a dramatic strength increment, sometimes denoted the *boot effect*, originating from trying to pull a boot out of mud. The investigation in this article will clarify if

this effect is present with the bucket foundation, which is expected. The development of pore pressure will furthermore be a function of the failure mechanism, a point where some uncertainties exist in the design methods.

2.2 Scaling Effects

In a model test consideration has to be taken, since the investigated phenomenon is a scaled down version of the real-life phenomenon. Using similarity laws along with continuum and fluid mechanics scaling parameters can be derived for the scaling of length, time, force, stress, velocity and time for both the sand and the pore water. The similarity laws state that both geometric, kinematic and dynamic similarity need to be obeyed, for the scaling to be correct. Often the dynamic similarity is the hardest to obtain, since it involves scaling of physical entities such as gravity and viscosity. (Larsen and Brorsen, 2009)

In the model of this article, the primary object is to investigate the influence of the loading velocity on the development of pore pressures and load bearing capacity under horizontal loading. The scaling of the sand and fluid is done without obeying the scaling laws, as e.g. the grain size in the sand is not scaled properly. The consequence of the wrong scaling is that the numerical values of the measured forces and pressures cannot be directly extrapolated from model to real size. This is however acceptable, since investigation of the nature of the phenomenons is the goal of this article.

3 Test Setup

The quality of the test setup is the key to achieve reliable results from any experiment, scaled or not. The tests described in this document are all scaled experiments performed in the pressure tank at Aalborg University. The reason that the experiments are performed in a pressure tank is that it is possible to apply a pressure, simulating that the foundation is situated below water and allowing a larger decrease in pore pressure before cavitation takes place. In the pressure tank at Aalborg University, it is possible to apply a maximum of 1000 kPa of pressure. An overview of the setup in the pressure tank is seen in figure 4.

3.1 Test Setup Overview

The test setup consists of multiple components which will be outlined in the following.

Actuator and Control System

The force is delivered from a hydraulic actuator which is controlled through a test control unit coupled with a computer. The actuator can be either displacement or force controlled. The actuator can deliver 100 kN of force, it has 500 mm of free range and a maximum velocity of at least 0.5 m/s. The movement of the actuator is controlled through a piece of computer software. In the software, it is possible to monitor movement of the actuator, force through a weight cell connected to the actuator and all the pressure transducers. The test control system also works as data acquisition software.

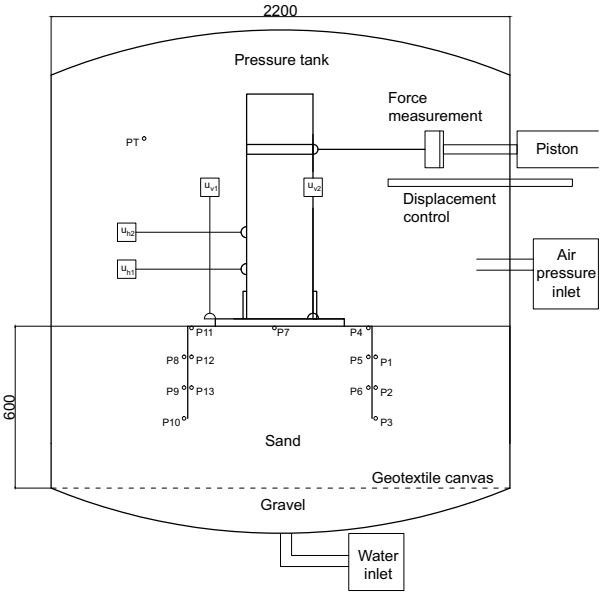

Figure 4: Overview of the pressure tank.

Bucket, Tower and Wire

The model bucket is made of stainless steel and has a diameter of 500 mm, a skirt length of 250 mm and a tower height of 610 mm, cf. figure 5. The tower is a galvanized RHS 180 $\times$ 100 mm steel profile reinforced at the bottom with two steel plates welded to the flanges. A round plate is mounted on the bottom of the tower to transfer the forces between the tower and the bucket lid via eight bolts. The model is a further development of a previous model, where the steel thickness of the skirt proved to be too small to withstand the development of earth pressures during the loading. In the new model the steel thickness is 10 mm in the lid and 5 mm in the skirt. Between the actuator and the piston a demountable steel wire is used to transfer the force. The whole setup is designed to be able to withstand a force of 100 kN at an eccentricity of 500 mm above the lid.

Measurements

13 pore pressures are measured on the bucket, cf. figure 5, to track the development during loading. Four displacement transducers are used to track the vertical, horizontal and rotational displacement. The displacement transducers are ASM wire transducers, which are carefully mounted before each test to ensure that the wire are respectively perfectly horizontal or vertical in the initial phase. The force applied via the piston is measured with a 100 kN force cell. The force cell is zeroed before

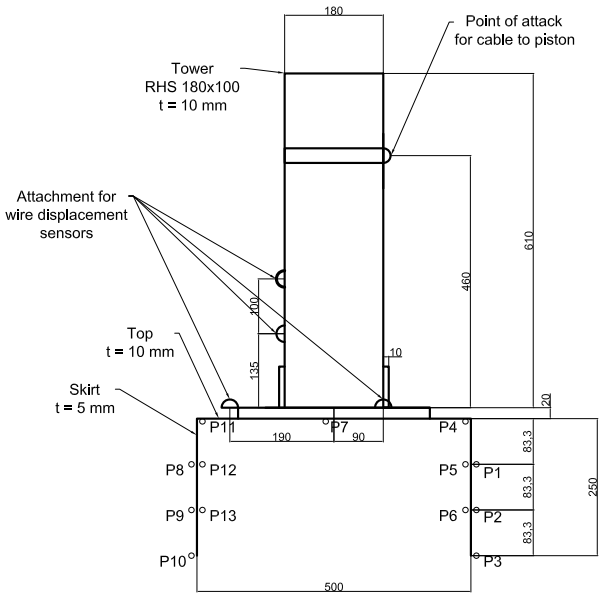

Figure 5: Sketch of the bucket.

each test is started, as it is affected by both the tightening of the wire and the pressure in the tank. This does to some degree cause the numerical value of the measured force to be wrong, but it is however comparable between the tests. The pressure in the tank is measured to ensure that the 200 kPa pressure is applied. The measurements are obtained using both the MOOG system and an older HBM Spider8 system, both are connected to a computer.

4 Preparation of Test Setup

Before each test is carried out a procedure for preparing the test setup is followed. The main purpose is to ensure that all the physical and geometrical parameters of the setup are identical in all the tests. The procedure has been investigated and documented in Fisker and Kromann (2004). The procedure is briefly explained in the following.

4.1 Preparation of Sand

The sand is prepared by following the points below,

1. Loosening of sand with water gradient
2. First vibration of sand
3. Second loosening of sand with water gradient
4. Second vibration of sand
5. Adjustment of water level in tank

The loosening of the sand is done by applying an upwards gradient of water, causing the effective stress in the sand to be reduced and thus loosening the grains from each other. The effective stress is calculated by,

$$\sigma' = (\gamma_m - \gamma_w \pm i\,\gamma_w)\,z, \tag{2}$$

where γ_m and γ_w are the unit weights of respectively sand and water, i is the gradient of water flow and z is the depth below the surface. As an upwards gradient of water flow is negative, the effective unit weight is reduced and the sand is loosened. A gradient of $i = 0.9$ is applied, which is equivalent to a pressure height difference of 0.54 m. The gradient is applied for a period of 5 minutes, whereafter the water surface in the tank is 5-10 cm above the sand surface. The following vibration is carried out using a vibrator rod that is lowered slowly into the sand until it is approximately 5 cm above the geotextile cover and then pulled slowly out. The slow velocity and the water layer above the sand surface minimizes the risk of creating air pockets in the sand. Before the leveling of the sand the water can be drained to make it easier to do, afterwards the water level is adjusted to approximately 6 cm above the sand.

4.2 CPT Testing

Prior to the installation of the model-bucket in the pressure tank CPT-tests are carried out in the prepared sand. This is done to ensure homogeneity in the soil volume. The tests are done using a mini-CPT cone, which is driven into the sand with constant velocity using a hydraulic piston. The CPT cone is mounted on an steel girder that can rotate 360° in the tank and allows for radial adjustment making CPT testing possible everywhere in the tank. Five CPT tests are done prior to each test at respectively the middle and at 90° intervals around the tank at 40 cm from the centre.

The sand in the tank is the Aalborg University Sand no. 1. This sand has been used extensively in the research at the Geotechnics Laboratory at Aalborg University, and its properties are thus very well documented. Using a series of triaxial tests performed with varying backpressure and relative density, a set of formulas has been derived to determine soil parameters from the cone resistance in a mini-CPT test (Ibsen et al., 2009). The following parameters can be determined from the CPT testing,

- Relative density I_D
- Angle of friction φ
- Angle of dilatency ψ
- Void ratio e
- Unit weight of the soil γ

The relative density is related to the cone resistance and the effective vertical in-situ stress through,

$$I_D = 5.14 \left(\frac{\sigma'_{v0}}{q_c^{0.75}} \right)^{-0.42}, \tag{3}$$

where σ'_{v0} is the effective vertical in-situ stress and q_c is the measured cone resistance. I_D is generally defined as,

$$I_D = \frac{e_{max} - e}{e_{max} - e_{min}}, \tag{4}$$

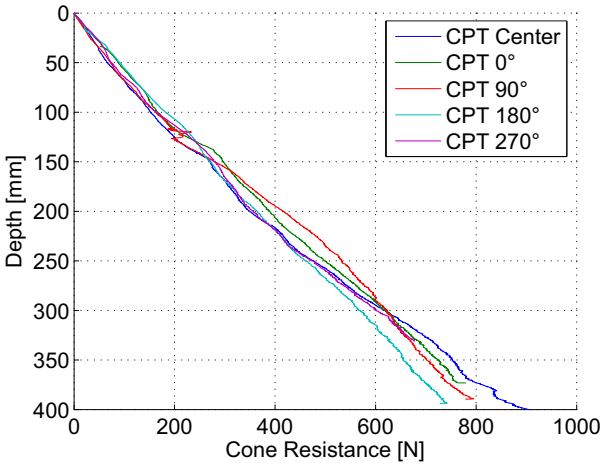

Figure 6: Cone resistance of five cone penetration tests.

with e_{max}, e_{min} and e as the maximum, minimum and current void ratios respectively. The effective in-situ stress can be found from the effective unit weight γ' and the depth z with,

$$\sigma'_{v0} = \gamma' \, z, \tag{5}$$

using the effective unit weight of the soil from,

$$\gamma' = \frac{d_s - 1}{1 + e}, \tag{6}$$

where d_s is the characteristic density of the soil equal to 2.64 for Aalborg University Sand no. 1. With the equations (3) to (6) an iterative procedure can be used to find γ', I_D and e. Empirical formulas to determine the triaxial angle of friction and dilatation fitted from a series of triaxial tests are seen in equations (7) and (8),

$$\varphi_{tr} = 0.152 \, I_D + 27.39 \left(\sigma'_{h0}\right)^{-0.2807} + 23.21, \tag{7}$$

$$\psi_{tr} = 0.195 \, I_D + 14.86 \left(\sigma'_{h0}\right)^{-0.09764} - 9.946, \tag{8}$$

where $\sigma'_{h0} = \sigma'_{v0} \; (1 - \sin(\varphi_{tr}))$, I_D is in percent and stresses are in kPa. With the presented set of formulas it is thus possible to achieve an estimate of specific soil parameters at each CPT location, which can be compared. Often the greatest difference will be present in the measure of relative density, where a difference between the CPTs of maximum 0.05 is accepted. If the difference is greater than 0.05 a third vibration procedure must be applied.

An example of the results of five CPT tests is shown in figure 6, where the cone resistance is plotted against the depth. During the preparation of the four tests presented in this article, some technical difficulties were encountered, meaning no usable CPT tests were done before test 2 and 3. Since the same preparation procedure has been used every time, and the results hereof have been good, the soil properties are assumed to be within the acceptable range. The results are thus treated similar for all tests.

Figure 7: Picture of the bucket ready for testing.

4.3 Installation of Bucket

When the sand is prepared and the CPT results are accepted, the bucket is installed in the centre of the tank using the hydraulic piston also used for the CPTs. The installation will cause disturbance in the sand volume, and is thus carried out step-wise to allow for dissipation of excess pore pressure to minimize the effects of the disturbance. As the speed of the installation piston is not changeable, the procedure is not optimal. It is however the same procedure for all tests, and should as such not have an influence on the validity of the results. Upon finishing the installation of the bucket all the measuring equipment is fitted and the horizontal hydraulic actuator is attached with a steel wire. The bucket equipped and ready for test can be seen in figure 7.

4.4 Applying Pressure to the Tank

After the installation the tank is sealed off and the compressor is set to 200 kPa of pressure relative to the atmospheric pressure. The build up of pressure is monitored with the MOOG system until an equilibrium at approximately 200 kPa is found and is then left overnight for the pressure state in the entire sand volume to stabilize. The test setup is thus fully prepared for testing.

Table 1: Overview of loading velocity for the tests.

Test no.	1	2	3	4
Velocity [mm/s]	0.10	1.00	10.0	100

5 Overview of Tests

A total of four successful tests are used for the results in the article. All of the tests are carried out with a horizontal displacement of the actuator of 150 mm applied at varying velocities. Table 1 shows the different test velocities. In the previous tests in Sjelmo et al. (2012) it was investigated if a very low loading rate (0.01 mm/s) behaved as drained condition, which was the case. A test with this loading rate is therefore not redone.

6 Results

In the following selected results from the four tests are shown. A very large quantity of data is produced in the tests, and only relevant results for underlining the points made are shown. All the test data is however treated, and the trend shown in this article is a picture of the general trends. Earlier analyses of similar tests have been made in Sjelmo et al. (2012) and Foglia et al. (2013), and these results will be compared with the new tests.

6.1 Force and Displacement

The recorded displacements v_1, v_2 and h_1 are all transformed to the resultant horizontal (H), vertical (V) and rotational (θ) displacements of the bucket with reference to the middle of the bucket lid. This reference point is used, as the actual rotation point of the bucket moves during loading and thus is not suitable. The procedure is iterative as the elongation of the wires in the transducers are influenced by all displacement components. In the iteration algorithm it is assumed that

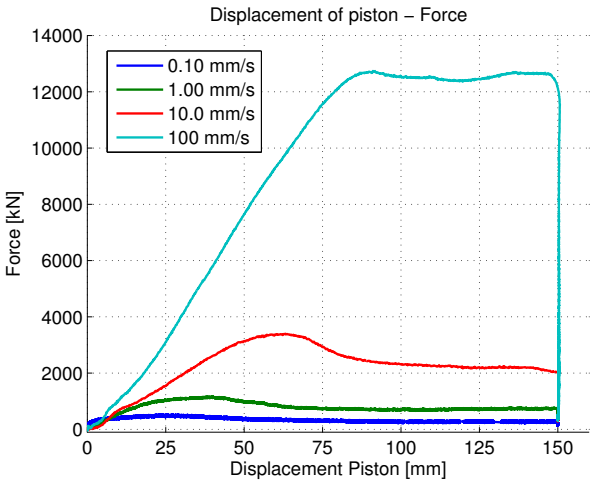

Figure 8: Force measurement as a function of the displacement of the piston.

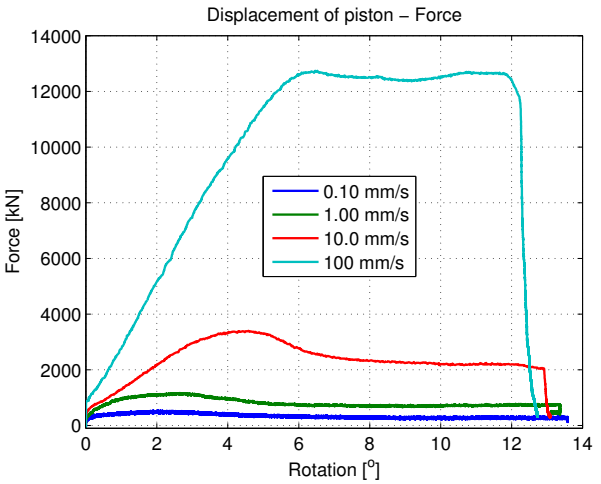

Figure 9: Force measurement as a function of the rotation of the bucket.

the displacements of the bucket can be divided into the three separate components that are mutually dependent on each other. The four monotonic loading tests differ only in loading velocity and consequently also duration. For all four tests the development of the force as a function of the actuator displacement and rotation of the bucket is shown in figures 8 and 9.

From the results it can be seen that as the displacement rate increases the measured necessary force to apply the displacement increases as well, which was expected. It is evident that the bearing capacity is highly rate dependent. In contrary to the previous tests done in Sjelmo et al. (2012), all the models have reached failure within the span of the displacement. While test 1, 2 and 3 reach an easily determinable peak, the fastest test 4 reaches a maximum force, which is then constant the rest of the loading phase. This indicates that the cavitation limit is reached at which no more capacity is available in the pore water. For all the tests the maximum force and the piston displacement and rotation of the bucket at the maximum points are shown in table 2. It is seen that the higher the displacement rate, the larger the rotation is before the maximum capacity is reached.

The vertical, horizontal and rotational displacement of the tests shown together with the force development is seen in figure 10. The difference between the resultant final horizontal displacement in the four tests is most pronounced, as it decreases with each increment in

Table 2: Maximum force, displacement of piston d_p and rotation θ of the bucket.

Test	Max Force [N]	d_p [mm]	θ [°]
0.10 mm/s	538.6	22.8	1.9
1.00 mm/s	1168.8	38.6	2.6
10.0 mm/s	3399.4	63.1	4.6
100 mm/s	12741.9	91.7	6.5

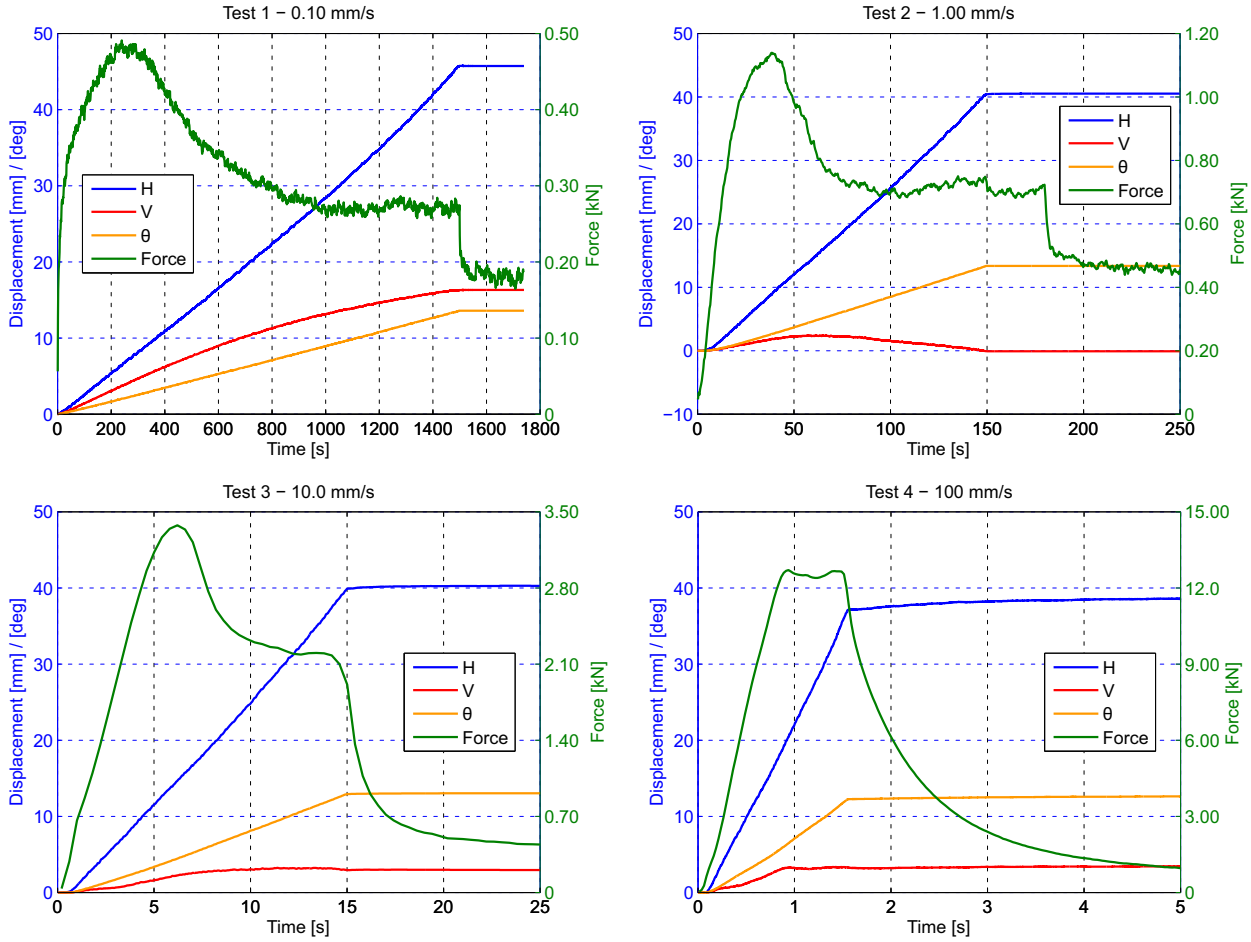

Figure 10: Displacement and force for all four tests. Test 2, 3 and 4 are zoomed in on the loading period.

the loading rate. The resultant vertical and rotational displacement also decrease with increasing loading rate, however the change here is not as large. In test 2 the vertical displacement first increases during the loading but then goes back to zero in the end of the loading. This effect is not clearly present in any of the other models, and can perhaps be a measurement error. Generally the displacements of the bucket decrease in magnitude as the loading rate increases. An explanation for this phenomenon is that the slower the loading rate, the easier it is for the pore water to dissipate, thus causing an increase in effective stresses which then cause a deformation in the soil. This effect is especially evident in test 1, as the vertical displacement here is very large compared to the other tests. The upwards vertical displacement is greatly influenced by the dissipation of negative pressure inside the bucket, i.e. pore water flowing from outside the bucket to the inside. With the low loading rate the change in pore pressure is almost balanced by the inflow of pore water.

6.2 Initial Stiffness

While it has been shown in the previous section that the lateral response of the bucket foundation is highly dependent on the loading rate when it comes to large displacements and ultimate capacities, it has earlier been shown, e.g. in Foglia et al. (2013) that the initial stiffness is independent on the loading rate. This is of interest, since the vast majority of the environmental loading will be small loads where the initial stiffness is important. The initial stiffness is furthermore interesting in dynamic investigation, which is however outside the scope

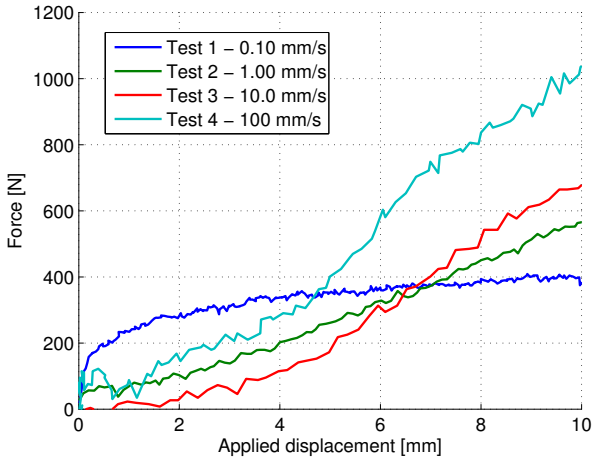

Figure 11: The force exerted in the first 10 mm of applied displacement.

of this article. The force exerted in the first 10 mm of applied displacement for all four tests is shown in figure 11. The response of test 1 is somewhat different than the other three tests, which is attributed to the very low loading rate. Tests 2-4 all show a very similar response for the first part of the applied displacement, with slopes of the force-displacement curve being similar. This is in good correlation with earlier findings, and the results from this article further verifies this phenomenon.

6.3 Pore Pressure Development

The pore pressure was recorded during all the tests in the locations shown in figure 5. As an example, the pore pressure development over time plotted together with the force development for test 3 is shown in figures 12 and 13. The pressure measurements are divided in the seven gauges inside of the bucket in figure 12 and the six gauges on the outside of the bucket in figure 13.

The build up of suction is as expected directly correlated with the applied force caused by the displacement. The build up is considerably larger inside the bucket, which is caused by flow-barrier effect from the impermeable skirt. A few of the pressure gauges show some irregularities in the results. This is namely P5 on the inside, which was expected to be somewhere between P4 and P6, and P7 which differ significantly from the two other gauges at the top P4 and P11. The irregularity in the results of P7 has been observed in all of the tests and could be caused by a slightly different method of instrumentation, as this gauge is placed directly under the mounting of the tower and therefore has a long and soft tube from the measuring point to the pressure transducer. Another, perhaps more likely, explanation is that the rotation point of the bucket is placed close to P7, causing the displacement of the bucket in this point to be smaller.

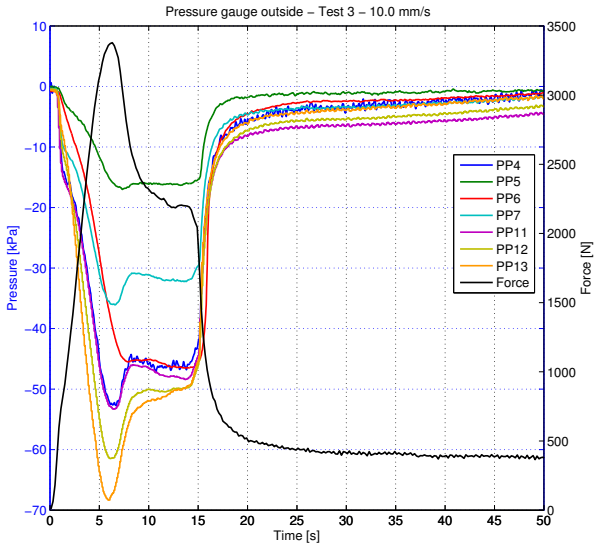

Figure 12: Pore pressure inside bucket during test 3.

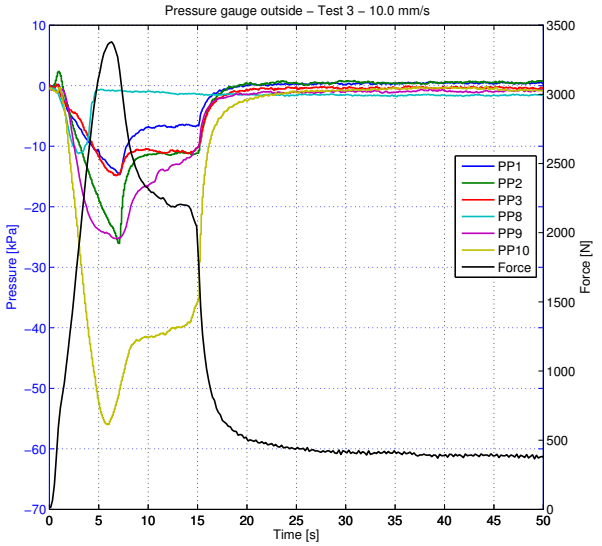

Figure 13: Pore pressure outside bucket during test 3.

The gauges away from the loading direction show the largest change in pressure, gauges P11, P12 and P13, however the top gauges P4 and P11 show very similar results, indicating a uniform pressure distribution on the lid if P7 is ignored. From the gauges on the outside, the trend is not as clear. The gauges closest to the surface P1 and P8 show the smallest pressure change, which is due to the very short drainage path.

From figure 10 it was shown that a significant strength increase takes place as the loading rate grows. This is an indication that while the drained condition might be suitable to calculate the capacity at low loading rates, it is not the case for a quite high loading rate. This is backed up by the results of test 3 examined in figure 12 and 13, which is not even the fastest loading rate.

The maximum pore pressure build up in all four tests is shown together in figures 14 to 16. The distribution on the lid, cf. figure 14 is similar in all four tests. The two side gauges P4 and P11 show almost the same maximum value, while P7 reaches only approximately 65 % of the maximum value in tests 2-4. As earlier pointed out, this could mean that the measurement is partly errorneus. In the execution of the tests problems with the P7 gauge occured, especially due to difficulties with fully saturating the transducer and connecting tube. Another conclusion is that the pressure distribution is not constant on the lid. In the tests done in Sjelmo et al. (2012) this phenomenon was not clearly visible.

The pressures along the back skirt, i.e. away from the loading direction, are seen in figure 15. These results can be compared to the results in Sjelmo et al. (2012), as the test setup herein had pressure gauges in the same positions on the back skirt. The outside pressures show a pressure distribution that is increasing non-linearly with the depth, which is consistent with previous results.

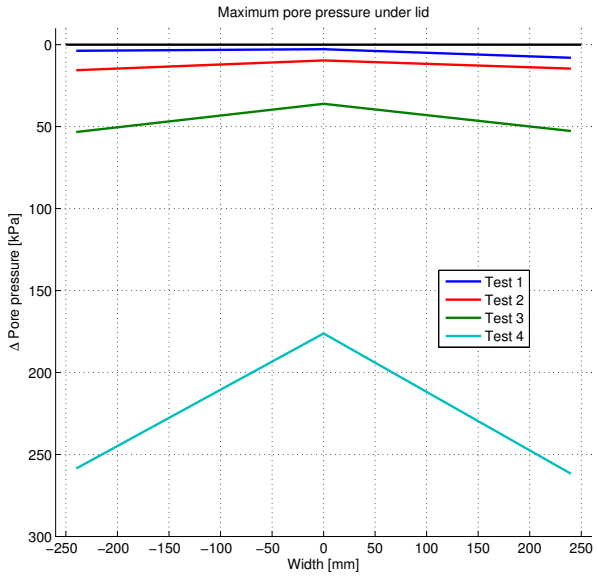

Figure 14: Force measurement as a function of the displacement of the piston.

The magnitude of the pressures significantly increases with the growth in loading rate as expected from the force measurements. The magnitude in the 100 mm/s test is 241.1 kPa at the bottom, which is below the cavitation limit. The fastest previous test was 10 mm/s, however this test did not show failure due to a very short loading distance, and the maximum pressures are thus not comparable.

The pressures on the inside of the back skirt are all larger than the corresponding pressures on the outside. Both the bottom point on the inside and outside are P10, as the pressure is recorded at the tip of the skirt. The pressure is slightly larger at P13 in all the tests, however a discontinuity in the pressure at P12 as found in Foglia et al. (2013) is not present. The pressure at P13 is the maximum measured pressure, which is close to the cavitation limit of approximate -290 kPa.

The pressures on the front skirt of the bucket, cf. figure 16, during loading have not been investigated earlier, and can therefore not be compared with previous results. The pressure on the outside is increasing with depth from P1 to P2, while the pressure at P3 is significantly lower. This could be caused by the rotation of the bucket, indicating the location of the rotation point being close in depth to P3. The pressures inside the front skirt follow a different trend compared to the back skirt. Firstly the magnitude of the pressures are smaller, but also a discontinuity is present at P5 2/3 up the skirt, before the pressure increases to that of the lid. As proposed in Foglia et al. (2013), a discontinuity could be caused by the drainage pattern.

In figure 17 the absolute pressure difference for P13 is shown for all four tests, with the time normalized with respect to the loading time. P13 is chosen since it shows the maximum measurements for all tests and it has one of the most distinct developments. For test 1 the response is very low, and can thus be considered almost completely drained. For test 2 and 3 an increment in pore pressure is seen, which does however become constant after respectively 0.2 and 0.4 of the normalized time. These tests can therefore be classified as partially drained, as the pore pressure cannot be increased indefinitely.

Test 4 shows an increase in pressure that is almost linear up to a plateau of around 275 kPa after which the increase is slightly slower. This test is therefore classified as substantially undrained, if not completely.

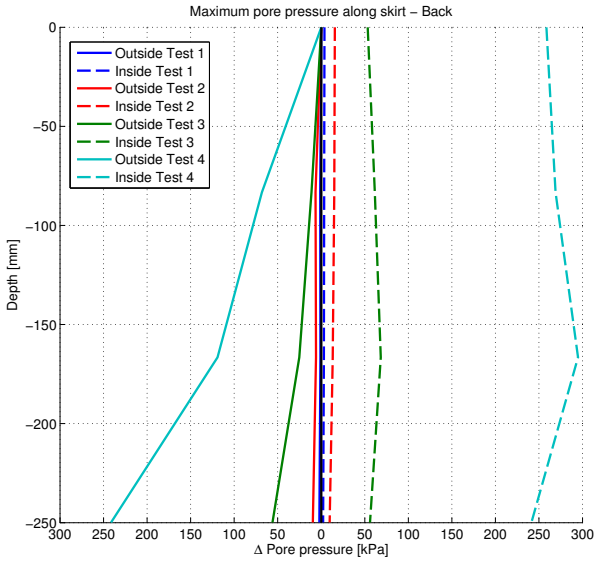

Figure 15: Force measurement as a function of the displacement of the piston.

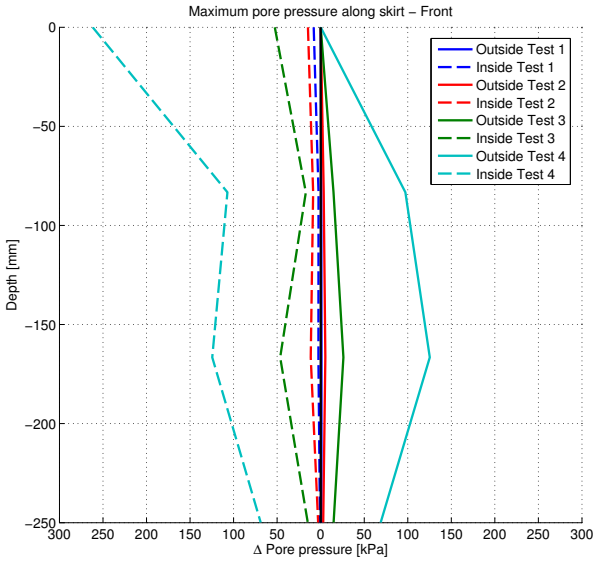

Figure 16: Force measurement as a function of the rotation of the bucket.

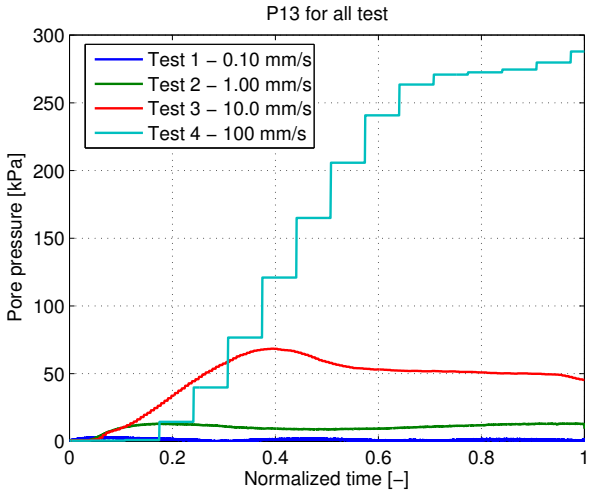

Figure 17: P4 for all tests with time normalized to loading time.

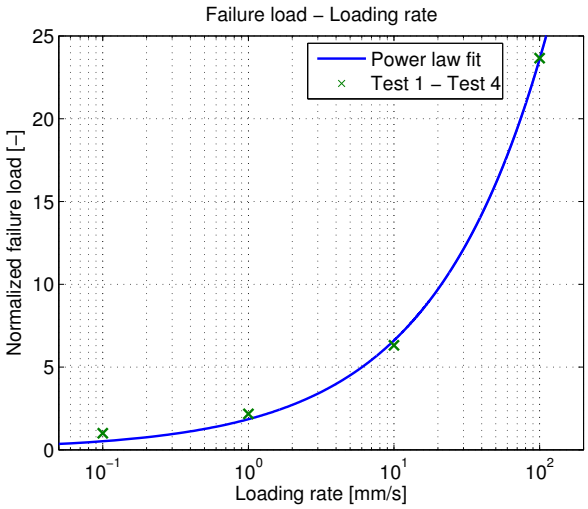

Figure 18: The normalized failure loading plotted against the loading rate.

The absolute value of the pressure is below the cavitation limit, however the decrease in slope indicates that the limit is close. For high loading rates and relatively large displacements the response can according to these results be classified as significantly more resistant to applied load than what the drained condition predicts.

6.4 Capacity as Function of Loading Rate

From the four different loading rates, it is investigated if the increase in ultimate capacity can be expressed with a mathematical expression. Firstly the failure load, cf. table 2, is normalized with the failure load of the slowest test, as it is assumed to be the drained capacity. A power function,

$$F_{\text{norm}} = a\, v_{\text{l}}^{b}, \tag{9}$$

where F_{norm} is the normalized force, v_{l} is the loading rate and a and b are fitting parameters, is fitted to the data points. The data points and the fit are seen in figure 18. It is evident that the development follows a power fit for the range of tests performed. It is expected that the strength increase reaches a plateau at around the level of the fastest test caused by the cavitation limit. Whether this is the case needs further investigation in future tests. The parameter of the fit is seen in table 3.

6.5 Non-dimensional Analysis

It was in Foglia et al. (2013) investigated whether the test results could be fitted to a non-dimensional function. The results are made non-dimensional by assuming a relationship,

$$\Delta p \propto \left(\frac{1}{k}\,,\, \frac{1}{T_{\text{L}}}\,,\, L_{\text{d}}\,,\, \gamma_{w} \right), \tag{10}$$

where k [m/s] is the permeability of the soil, T_{L} [s] is the loading period, L_{d} [m] is the drainage length assumed proportional to the skirt length L and γ_{w} [N/m^3] is the unit weight of the soil. While the loading period T_{L}, and the unit of it, is a term from dynamic loading, it is assumed that the loading rate can be used instead, despite having a wrong unit. The non-dimensional group is thus,

$$\frac{\Delta p}{\gamma_{\text{w}}\, L} = f\left(\frac{L}{k\, T_{\text{L}}} \right). \tag{11}$$

The function f is unknown, and a fit with a power function is examined,

$$\frac{\Delta p}{\gamma_{\text{w}}\, L} = c\, \left(\frac{L}{k\, T_{\text{L}}} \right)^{d}. \tag{12}$$

With the parameters c and d being fitting parameters. The data from pressure gauges P4 and P11 are used, since these gauges show the maximum response under the lid. For each of the four tests the maximum value is chosen from the dataset, making the non-dimensional group an expression of the maximum obtained pressure difference for a given soil, loading rate and geometry. With the two gauges chosen there are thus eight data points in total with four different loading rates. In figure 19 the data points are shown together with the fitted function. The fitted parameters are seen in table 3. The fitted power law follows the data points quite good and is somewhat an indication that a function of this type is suitable. More test data should be used before a final function can be fitted to the data.

7 Conclusion

The new test equipment in the pressure tank has been implemented and four successful tests have been executed. The displacement rates used ranged from 0.1

Table 3: The fitted parameters of equations (9) and (12).

a	b	c	d
1.848	0.553	$1.033 \cdot 10^{5}$	-0.654

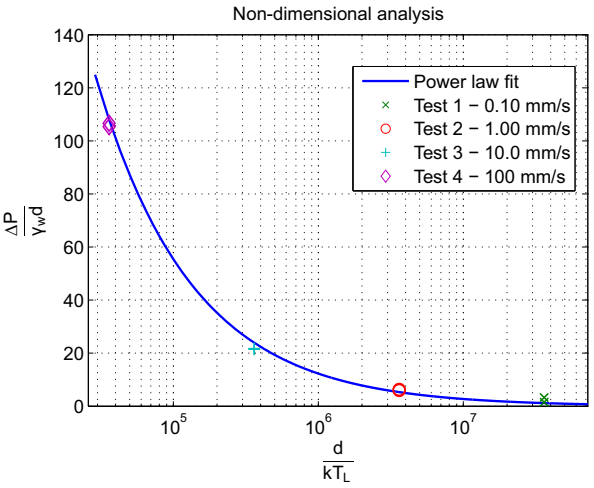

Figure 19: Non-dimensional analysis of maximum pore pressure development.

mm/s to 100 mm/s. The results showed a significant increase in the bearing capacity from approximate 0.5 kN in the slowest test to 12.7 kN in the fastest test. From the displacements gauges it was seen that the overall displacement of the bucket foundation decreased as the loading rate increased. An explanation for this is the lack of sufficient seepage of pore water allowing for deformations with the fast loading rates.

The pore pressure development was tracked by 13 pressure gauges during all four tests. For the slowest test a very low pore pressure change occurred, indicating almost fully drained conditions. As the loading rate increased, the measured pore pressures increased, indicating partially undrained conditions. For the fastest tests the build up of pore pressures increased throughout the entire loading sequence pointing to substantially undrained conditions. There was a clear correlation between the faster loading rates, the build up of pore pressures and the rise in lateral capacity of the foundation.

The pressure distribution of the bucket foundation was found to be similar to earlier investigations, albeit without a discontinuity on the inside of the back skirt. The shape of the distribution was almost identical in all four tests, further proving the reliability of the results. All gauges showed a negative development of pore pressure, meaning suction occurred around the entire bucket under loading.

The initial stiffness of the lateral response was investigated by looking at the first 10 mm of applied displacement. Apart from the slowest test all tests showed a similar response with similar slopes of the force-displacement curve. This proves earlier findings, where the initial stiffness has been found to be independent on the loading rate.

The capacity of the bucket foundation increased with the loading rate in a manner that could be fitted with a power law, more test data is needed to determine whether this trend continues beyond the test rates of this article. Lastly the results from two of the pressure gauges were analyzed using a non-dimensional group. It was found that the development of pore pressures can also be described using a power law, although more test data with different geometries is needed to improve the reliability of the findings.

Overall the initial thesis of the article proved to be verified by all the findings in the treatment of the results.

8 Further Work

The results put forward in this article are a product of the very first tests with the new test-setup in the pressure tank at the Geotechnics Laboratory at Aalborg University. During the work in the laboratory several useful experiences with the setup and new equipment were made, which continuously leads to optimization of the whole setup. In time this will lead to better tests, which can further validate the points presented in this article.

During the analysis of the test results it was found that the signals from the transducers were polluted with noise to a quite large degree. The noise present was of varying amplitude for the various signals, and could indicate problems with the wiring and soldering of the cables and plugs. Further work could involve trying to minimize this noise.

The tests 1 to 4 showed in the article are all done with a foundation with $L/D = 0.5$. Further work in the laboratory involves similar testing with suction buckets of other dimensions, already now tests with a $L/D = 1.0$ bucket are planned. Furthermore the test setup is able to handle cyclic loading and two-way loading, which can further be used to analyze the behaviour of the suction bucket foundation type.

References

Fisker and Kromann, **2004**. L.B. Fisker and K. Kromann. *Cyklisk Belastning af Bøttefundament i Tryktank - Speciale*, 2004.

Foglia, Ibsen, Nielsen, and Mikalauskas, **2013**. A. Foglia, L.B. Ibsen, S.K. Nielsen, and L. Mikalauskas. *A Preliminary Study on Bucket Foundations under Transient Lateral Loading*. 2013.

Ibsen, Hanson, Hjort, and Thaarup, **2009**. Lars Bo Ibsen, M. Hanson, T. Hjort, and M. Thaarup. *MC-Parameter Calibration for Baskarp Sand No. 15*. 2009.

Ibsen and Lade, **1997**. L.B. Ibsen and P.V. Lade. *A study of the phase transformation and the characteristic lines of sand behavior*. 1997.

Ibsen and Lade, **1998**. L.B. Ibsen and P.V. Lade. *The Role of the Characteristic Line in Static Soil Behavior*. 1998.

Larsen and Brorsen, **2009**. Torben Larsen and Michael Brorsen. *Lærebog i Hydraulik*. 978-87-7307-691-0. Aalborg Universitetsforlag, 2009.

Nielsen, Ibsen, Sørensen, and Shajarati, **2013**. Søren Kjær Nielsen, Lars Bo Ibsen, Kris Wessel Sørensen, and Amir Shajarati. *Undrained Cyclic Behaviour of Dense Frederikshavn Sand*. 2013.

Sjelmo, Mikalauskas, Ibsen, and Foglia, **2012**. Å. Sjelmo, L. Mikalauskas, L.B. Ibsen, and A. Foglia. *Soil-Structure Interaction in Cohesionless Soils due to Monotonic Loading*. 2012.

Universal Foundation A/S, **2013**. Universal Foundation A/S. *Press material*. URL: `http://www.universalfoundation.dk/en/press/10/7/5`, 2013. Downloaded: 29-05-2013.

Recent publications in the DCE Technical Memorandum Series

DCE Technical Memorandum no. 31, Determination of p-y Curves for Bucket Foundations in Sand Using Finite Element Modeling, Bjørn Staghøj Knudsen, Martin Underlin Østergaard, Lars Bo Ibsen and Johan Clausen, June 2013.

DCE Technical Memorandum no. 32, Implementation of a Stress-dependent Strength Material Model in PLAXIS 3D, Bjørn Staghøj Knudsen, Martin Underlin Østergaard and Johan Clausen, June 2013.

DCE Technical Memorandum no. 33, Small-scale Testing of Bucket Foundations in Sand, Bjørn Staghøj Knudsen, Martin Underlin Østergaard and Lars Bo Ibsen, June 2013.

ISSN 1901-7278
DCE Technical Memorandum No. 33